

The geomagnetic variation anomaly in the northern Pyrenees: study of the temporal variation

G. Vasseur, K. Babour, Michel Menvielle, Jean-Claude Rossignol

► **To cite this version:**

G. Vasseur, K. Babour, Michel Menvielle, Jean-Claude Rossignol. The geomagnetic variation anomaly in the northern Pyrenees: study of the temporal variation. *Geophysical Journal International*, Oxford University Press (OUP), 1977, 49 (3), pp.593-607. 10.1111/j.1365-246X.1977.tb01306.x . insu-02155799

HAL Id: insu-02155799

<https://hal-insu.archives-ouvertes.fr/insu-02155799>

Submitted on 30 Jul 2020

HAL is a multi-disciplinary open access archive for the deposit and dissemination of scientific research documents, whether they are published or not. The documents may come from teaching and research institutions in France or abroad, or from public or private research centers.

L'archive ouverte pluridisciplinaire **HAL**, est destinée au dépôt et à la diffusion de documents scientifiques de niveau recherche, publiés ou non, émanant des établissements d'enseignement et de recherche français ou étrangers, des laboratoires publics ou privés.

The geomagnetic variation anomaly in the northern Pyrenees: study of the temporal variation

G. Vasseur *Centre Géologique et Géophysique – USTL, Place E' Bataillon, 34060 Montpellier Cedex, France*

K. Babour *Centre de Recherches Géophysiques, Laboratoire de Géomagnétisme, 24, rue Lhomond, 75231 Paris Cedex 05, France*

M. Menvielle and J. C. Rossignol *Institut de Physique du Globe, 4, Place Jussieu, 75230 Paris Cedex 05, France*

Received 1976 October 29; in original form 1976 July 14

Summary. The existence and the spatial properties of an important geomagnetic anomaly in the north of the eastern part of the Pyrenees have been described in a previous paper of this journal (Babour *et al.*). The temporal dependance of the anomalous magnetic field and its relation with the normal field is now studied. Due to its remarkable property – separation of spatial and temporal variations – only one component of the anomalous field at one station needs to be considered. A high coherency between the variations of the anomalous field and those of the normal field projected in the direction 40° E of north is found. Transfer functions are obtained in the frequency domain and also directly in the time domain using two different methods. The various estimates of the transfer function are in good agreement for the period range 20 min–2 hr. As the anomaly is due to a concentration of currents induced elsewhere, the obtained transfer function is interpreted in terms of a non-local relation associated with the area where the induction takes place which is identified with oceanic regions. Using reasonable assumptions, the transfer function is shown to be connected to the ratio of the electric to magnetic field over oceanic areas. The existence of a highly conducting medium at 50 km depth is proposed. The mechanism responsible for the concentration of currents is qualitatively discussed in relation with the geometry of continental margins.

1 Introduction

1.1 SUMMARY OF PREVIOUS RESULTS

In a previous paper (Babour *et al.* 1976), we have presented the results of a set of geomagnetic experiments carried out in the north of the eastern part of the Pyrenees (Fig. 1). In

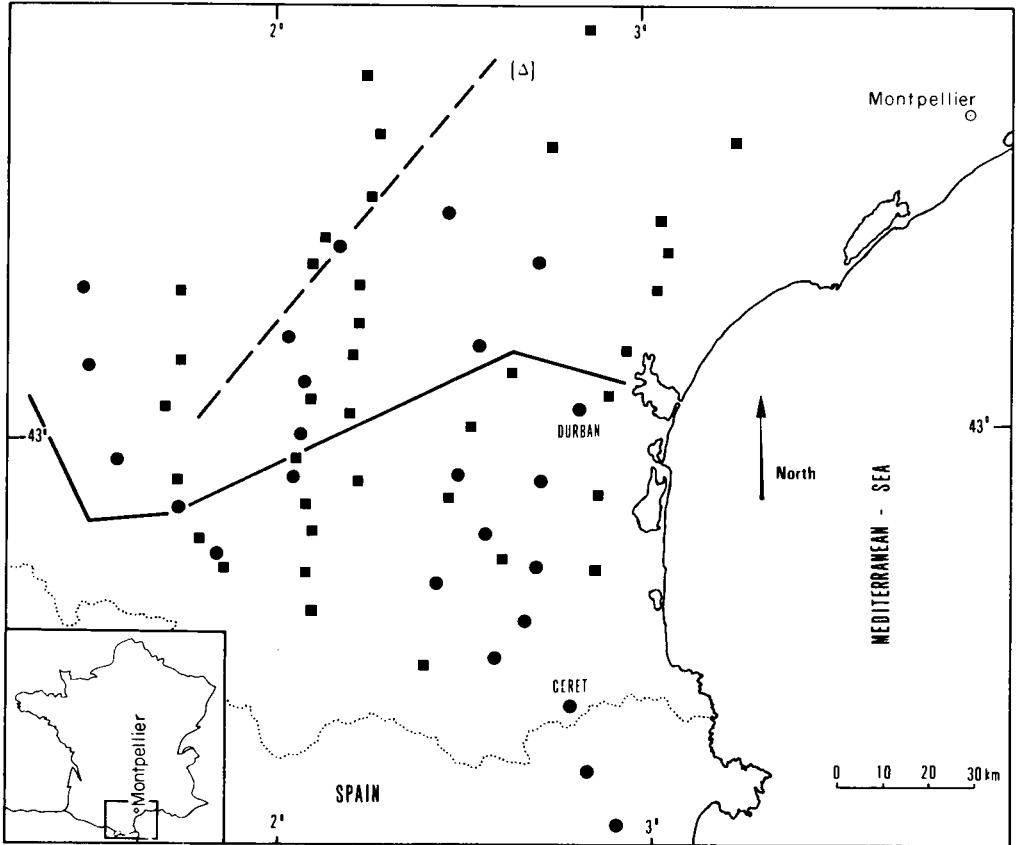


Figure 1. Location of the stations occupied from 1972 to 1975 in the eastern part of the northern Pyrenees. The full broken line represents the trend of the geomagnetic anomaly and the dashed line (Δ) is the direction most effective for induction. Round: Mosnier variometers; square: Askania.

the studied area, a geomagnetic anomaly has been found by investigating the differences between the time variations of the field recorded in the various stations and the time variations of the field simultaneously recorded in a reference station. As discussed in the previous paper, this reference station – Ceret (Fig. 1) – is considered as a normal one since it is located in an area where the horizontal field has been found homogeneous. Therefore the differences of the horizontal field are identified with the horizontal components of the anomalous field. This geomagnetic anomaly whose trend is sketched on Fig. 1 is a very strong one: the variations of the horizontal anomalous field $H_a(t)$ and those of the normal field can have comparable amplitudes in the vicinity of the maximum of the anomaly. Furthermore, it has been pointed out (Babour *et al.* 1976) that the anomaly has a fixed geometry independent of the period for magnetic variations of period greater than 10 min. This property is valid for any type and any amplitude of disturbance; it implies that the anomalous field is the product of a function of time $R(t)$ by a function of space $h_a(P)$

$$H_a(P, t) = h_a(P) \cdot R(t). \quad (1)$$

This property has been checked in the time domain by the similarity which exists between any two components ($\Phi(t)$ and $\Psi(t)$) of the anomalous field observed simultaneously either in two different stations or in the same station. In the frequency domain,

this property implies a linear relationship between the Fourier components of $\Phi(t)$ and $\Psi(t)$. This can be shown by studying the coherency between $\Phi(t)$ and $\Psi(t)$ defined by

$$C(f) = [(|S_{\Phi\Psi}|^2)/(S_{\Phi\Phi} \cdot S_{\Psi\Psi})]^{1/2}. \quad (2)$$

$S_{\Phi\Phi}$ and $S_{\Psi\Psi}$ being the power spectrum of Φ and Ψ respectively, $S_{\Phi\Psi}$ being their cross spectrum. For all the cases, $C(f)$ is greater than 0.92 for periods over 600 s and the imaginary part of $S_{\Phi\Psi}$ is less than 1 per cent of the real part. These two properties prove, in the frequency domain, that the components Φ and Ψ are proportional.

The character of the electric currents responsible for the anomaly was previously discussed (Babour *et al.* 1976). The large amplitude of the anomalous field and its property (equation 1) imply that these currents are not locally induced in some elongated conducting structure; instead of that, the anomaly is due to currents induced in large surrounding areas and locally channelled. Therefore the function $R(t)$ must be linearly related to the normal field in the area where these currents are induced.

1.2 PURPOSE OF THE PRESENT WORK

The previous paper dealt with the study of the spatial dependence of the anomalous field — $h_a(P)$. The purpose of this paper is to study the relation between the time variations of the anomalous field $R(t)$ and those of the normal field, using various methods.

At mid-latitude and for the magnetic events that we have studied — bay type variations — the external field can be considered as uniform over horizontal distances of several hundred kilometres (Rikitake 1966); the vertical component of the normal field is then small compared to its horizontal components. Therefore, it can be assumed that the variations of the normal field in the area where induction occurs and those of the normal field near the anomaly are identical, although the location of the area where induction occurs is largely unknown. Thus a relationship between the variations of the anomalous field and those of the normal field simultaneously recorded outside the anomaly should be studied.

The approach which is the most commonly used for the study of geomagnetic anomalies, is the computation in the frequency domain of transfer functions between the variations of the *vertical component* Z of the geomagnetic field and those of the horizontal component of the normal geomagnetic field. Thus, it is assumed that the vertical component Z in the anomalous area is entirely anomalous — or at least that its normal part does not correlate with the normal horizontal field. For the present study, the experimental method used (Babour & Mosnier 1976), provides — with a good accuracy — the *horizontal component* of the anomalous field. Furthermore, the relation (1) allows one to compare the variations of *one component* of the anomalous field — $R(t)$ — recorded in *one station* to the simultaneous variations of the field $H_n(t)$ recorded at the reference station assumed to be a normal one.

We have chosen for $R(t)$ the north–south component of the anomalous field at the Durban station (*cf.* Fig. 1) — located near the maximum of the anomaly — and for $H_n(t)$, the field recorded at the Ceret station as discussed in the first paragraph. We have selected three samples during which large variations of the field occur — several tens of gammas on the normal field — and without preferential direction of polarization. The characteristics of these events are described in Table 1.

These three events have been used to look for the relationship between the variations of the anomalous field $R(t)$ and those of the normal horizontal field $H_n(t)$. This relationship will be first studied in the frequency domain and then in the time domain. The results will be compared and interpreted.

Table 1.

| No. | Beginning | End |
|-----|------------------------|-------------------|
| 1 | 1973 Oct. 5 18 h L.T. | Oct. 6 02 h L.T. |
| 2 | 1975 Oct. 8 18 h L.T. | Oct. 9 06 h L.T. |
| 3 | 1974 Oct. 17 18 h L.T. | Oct. 18 02 h L.T. |

2 Analysis in the frequency domain

2.1 SPECTRAL ESTIMATES

In order to obtain a good estimate of the power spectra for periods less than 1 or 2 hr, the data were filtered using a high pass filter with a cut-off period of 7200 s. The filters used are Butterworth recursive filters (Souriau 1974); they provide an attenuation of 0.5 for the cut-off period and an attenuation rate of 36 dB/octave. The auto- and cross-covariance functions were then computed and multiplied by a Parzen window of half-width 3000 s (Jenkins & Watts 1968). Finally, taking the Fourier transform of these functions, we have obtained an estimate of the spectra with a frequency interval of 1.67×10^{-4} Hz.

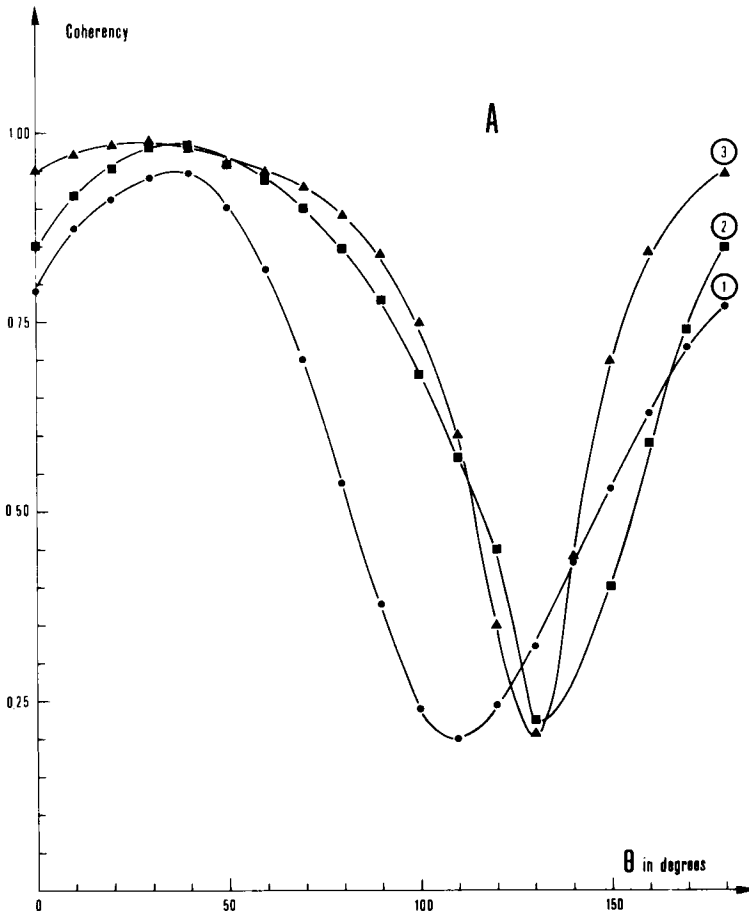


Figure 2 (a)

Figure 2. Variation with θ of the coherency between the anomalous field $R(t)$ and the normal horizontal field projected upon the direction θ : $H_n, \theta(t) = H_n \cos \theta + D_n \sin \theta$ ($0^\circ \leq \theta \leq 180^\circ$). Cases A, B, C correspond to samples 1, 2 and 3; on each figure the following period bands are considered: 1 – period band 2000–6000 s; 2 – period band 1200–2000 s; 3 – period band 900–1200 s.

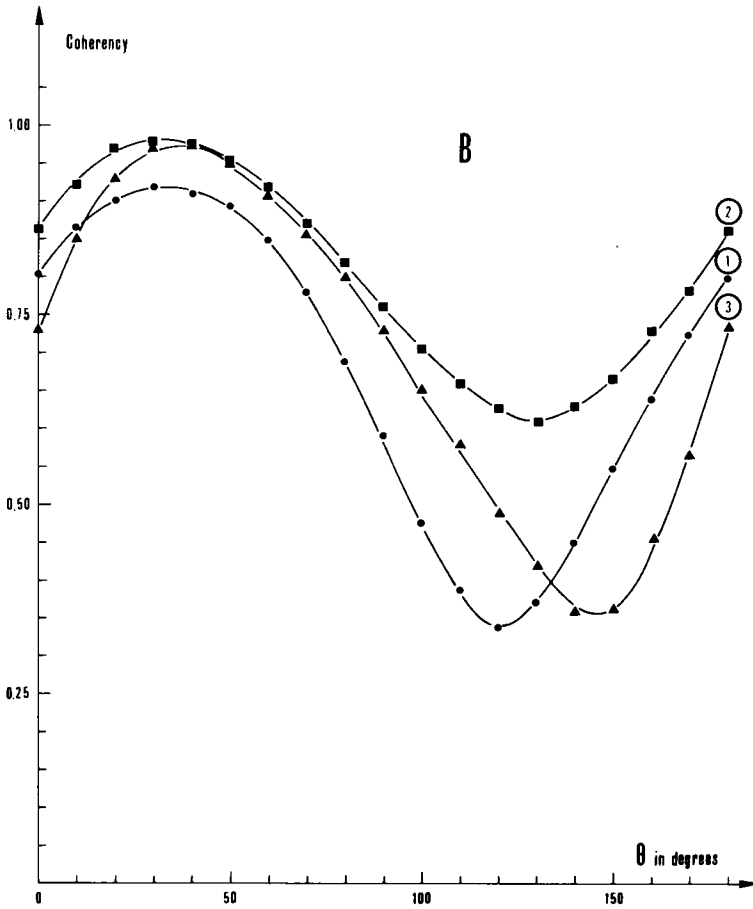


Figure 2 (b)

2.2 DIRECTION MOST EFFECTIVE FOR INDUCTION

To find the direction most effective for induction, i.e. the direction (Δ) along which the coherency between the normal and the anomalous field is maximum, the coherency – defined by (2) – between $R(t)$ and the normal horizontal field projected on the direction of the unit vector u_θ has been computed (Fig. 2). θ is the angle between the magnetic north and u , positive to the east. An obvious maximum of coherency – greater than 0.82 for all the samples and for all the period range under study – occurs around $\theta = 40^\circ$ E of north. Thus the direction 40° E of north is the one where induction is most effective for the observed anomaly.

In addition, the cross spectrum between $R(t)$ and $H_{n,40^\circ}(t)$ has an imaginary part which is relatively large compared to its real part, i.e. there is a phase shift between $R(t)$ and $H_{n,40^\circ}(t)$.

2.3 TRANSFER FUNCTIONS

Let $\tilde{H}(f)$ and $\tilde{D}(f)$ be the Fourier transforms of the north–south and east–west components of the normal horizontal field $H_n(t)$ and $\tilde{R}(f)$ that of $R(t)$. The real coefficients $a_H(f)$, $b_H(f)$, $a_D(f)$, $b_D(f)$ of the transfer function are those which minimize the residual

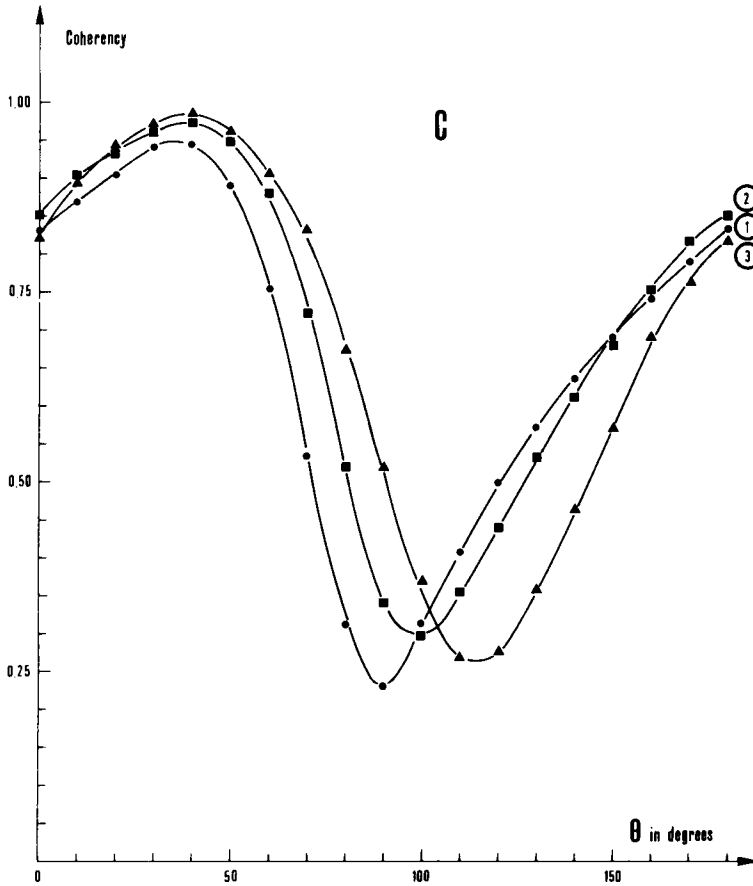


Figure 2 (c)

power $|\delta\tilde{R}|^2$ in the following equation

$$\tilde{R} = (a_H + ib_H)\tilde{H} + (a_D + ib_D)\tilde{D} + \delta\tilde{R}. \quad (3)$$

This transfer function is usually characterized (Schmucker 1970; Cochrane & Hyndman 1970) by the in-phase vector $\mathbf{A}(f)$ and the out-of-phase vector $\mathbf{B}(f)$ whose components are respectively $(-a_H, -a_D)$, (b_H, b_D) . Fig. 3 shows the modulus of the vectors as well as their direction with respect to the magnetic north – these directions being positive toward the east. The directions of vectors \mathbf{A} and \mathbf{B} obtained with the three samples are in reasonable agreement; moreover, the vectors \mathbf{A} and \mathbf{B} have roughly the same direction: 40° E of north. This result expresses in a different way the previous result (Fig. 2). The moduli $|\mathbf{A}|$ and $|\mathbf{B}|$ are also comparable among individual samples. For period less than 900 s, $|\mathbf{A}|$ is greater than 1, i.e. the anomalous field considered is greater than the normal one. The ratio $|\mathbf{A}|/|\mathbf{B}|$ varies from 0.25 to 0.5 when the period varies from 600 to 5400 s; so the phase shift between normal and anomalous field increases with the period.

3 Analysis in the time domain

The study of the relationship between the anomalous field and the normal one is now carried out directly in the time domain; this study can be started in, mainly because of the characteristics of the experimental equipment which allows to obtain the various fields with

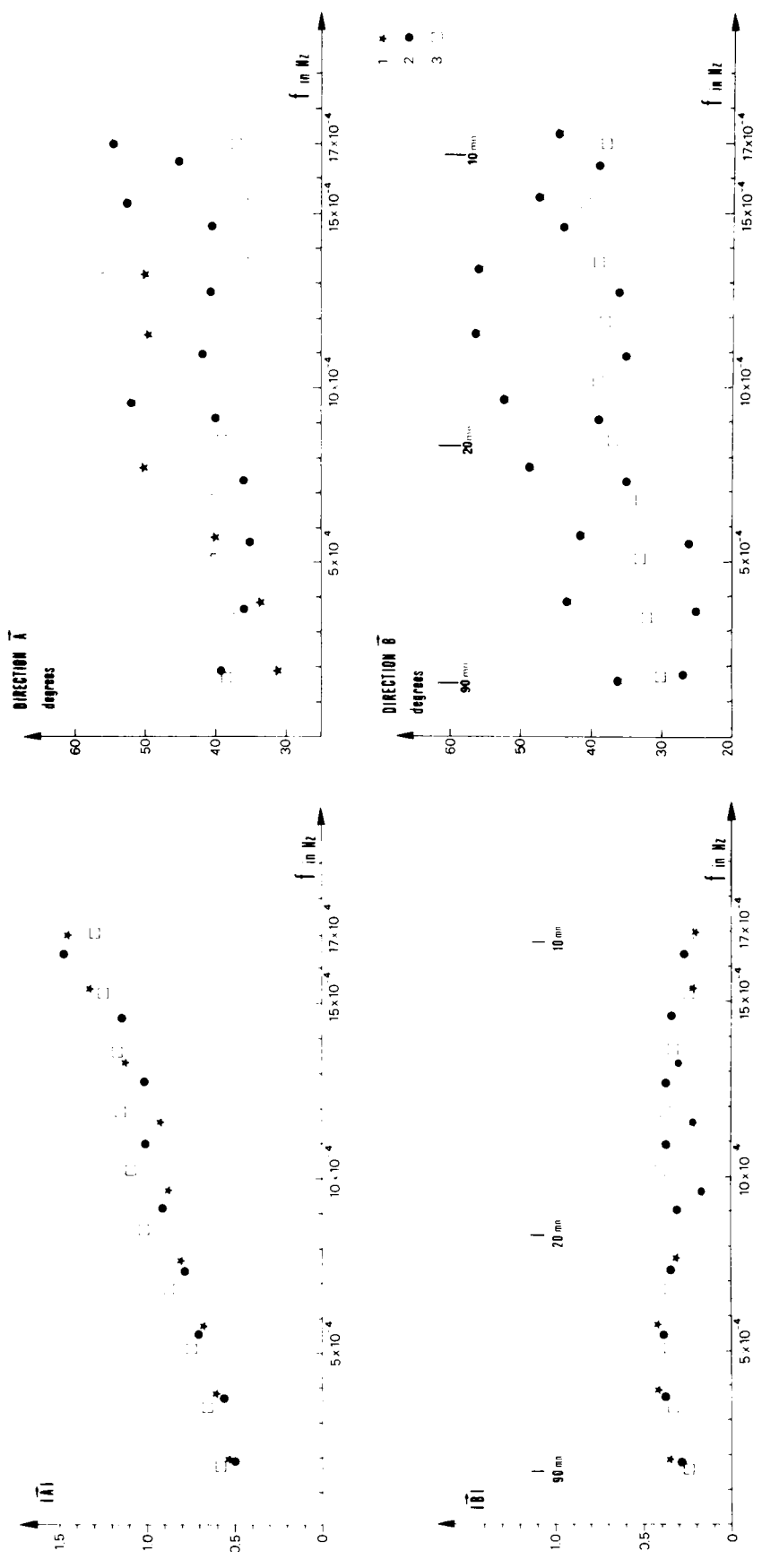


Figure 3. On the left part: modulus of the in phase $|A|$ and out of phase $|B|$ induction vectors as a function of frequency for three samples. On the right part: direction in degree of the vectors **A** and **B** with respect to the magnetic north (positive to the east).

a good accuracy: differences measured in real time with high stability and low noise sensors (Babour & Mosnier 1976). Therefore the impulse response of the convolution filter which transforms the normal field $\mathbf{H}_n(t)$ into the anomalous one $R(t)$ has been calculated. This filter is equivalent in the time domain to the transfer function in the frequency domain. The impulse response of this linear filter has been found out by two different ways: (i) using the discrete Wiener filter formulation; (ii) assuming that the behaviour of the linear filter which yields $R(t)$ from $\mathbf{H}_n(t)$, may be described by a linear differential equation and by computing the coefficients of this equation.

3.1 DETERMINATION OF THE WIENER FILTER

Let $X(t)$ be the projection of $\mathbf{H}_n(t)$ on the direction (Δ) most effective for induction (40° E of north, cf. Section 2). $R(t)$ is supposed to be linearly related to $X(t)$ by

$$R(t) = \int_0^\infty h(u) X(t-u) du + \delta R(t) \quad (4)$$

where $h(t)$ is the impulse response of the linear filter assumed to be physically realizable (i.e. its impulse response is causal: $h(t) = 0$ when $t < 0$) and $\delta R(t)$ is a residual. Minimizing the average power of this residual leads to the well known Wiener–Hopf integral equation

$$\gamma_{XR}(t) = \int_0^\infty h(u) \gamma_{XX}(t-u) du \quad (5)$$

where $\gamma_{XX}(t)$ and $\gamma_{XR}(t)$ are respectively the autocovariance and cross covariance functions of $X(t)$ and $R(t)$. For discrete time series ($t = nT$ where n is an integer-valued index and T the sample rate), the discrete operator (h_n , $n = 1, 2, \dots, N$) corresponding to $h(t)$ must satisfy a system of equations (Treitel & Robinson 1966)

$$\sum_{n=0}^N h_n c_{nm} = d_m, \quad m = 0, 1, \dots, M \quad (6)$$

with $c_{nm} = \gamma_{XX}(n-m)T$ and $d_m = \gamma_{XR}(mT)M+1$ is the number of equations considered. The number of coefficients h_n is arbitrarily limited to $N+1$ non-zero values. Let \mathbf{C} be the matrix $[c_{nm}]$, \mathbf{d} and \mathbf{h} the vectors $[d_m]$ and $[h_n]$. In the case $M > N$, the system (6) is over-constrained; it can be solved using least-square techniques, i.e. by minimizing the value of $\|\mathbf{C} \cdot \mathbf{h} - \mathbf{d}\|$. However, the solution obtained presents large oscillations; this instability is due to the bad conditioning of the matrix \mathbf{C} . It is possible to eliminate this instability by introducing an approximate solution \mathbf{h}^0 and by minimizing $\|\mathbf{C} \cdot \mathbf{h} - \mathbf{d}\| + \lambda \|\mathbf{h} - \mathbf{h}^0\|$, where λ is a positive parameter. The greater λ is chosen, the smaller $\|\mathbf{h} - \mathbf{h}^0\|$ will be. In fact, a very small value of λ – less than $1/100$ of the diagonal elements of \mathbf{C} – is enough to obtain a stable solution. For the value of \mathbf{h}^0 , a simple proportionality between $X(t)$ and $R(t)$ was chosen, using the similarity between these two time series (this similarity can be noticed on Fig. 5). Tests have indicated that the resulting solution \mathbf{h} is relatively independent of the choice of \mathbf{h}^0 .

Fig. 4 gives the impulse responses obtained for the three samples with $T \approx 120$ s, $M = 35$ and $N = 30$ (maximum delay ≈ 60 mn): the three curves are very close one to another.

Using the arithmetic average of these three estimates, a mean impulse response can be calculated. In order to obtain a predicted output $R'(t)$ and to compare it to the actual series $R(t)$, the input $X(t)$ is convolved with this mean impulse response. An example of this com-

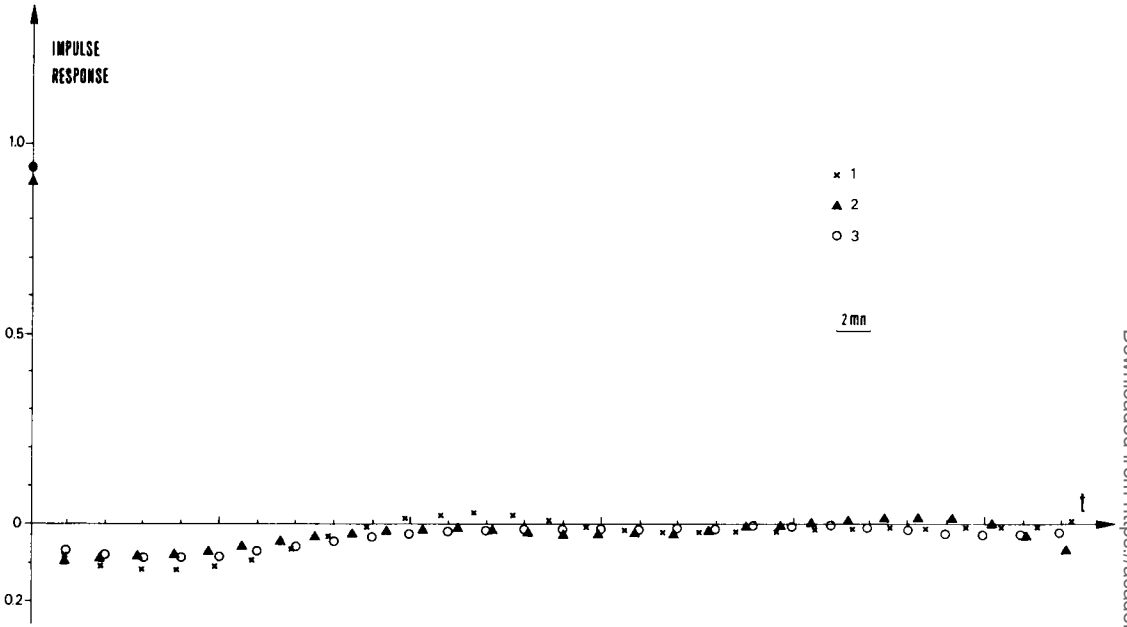


Figure 4. Impulse response of the discrete Wiener filter obtained with the three samples 1, 2 and 3 as a function of the delay.

parison is shown on Fig. 5 and shows a good agreement, except for a discrepancy for the highest frequencies.

3.2 COMPUTATION OF THE COEFFICIENTS OF A DIFFERENTIAL EQUATION

Another direction of investigation is to estimate a simple dynamic model equivalent to the linear system relating the anomalous field to the normal one. We may assume that the system is governed by the simple differential equation, similar to the equation for the intensity in a resistance–inductance circuit:

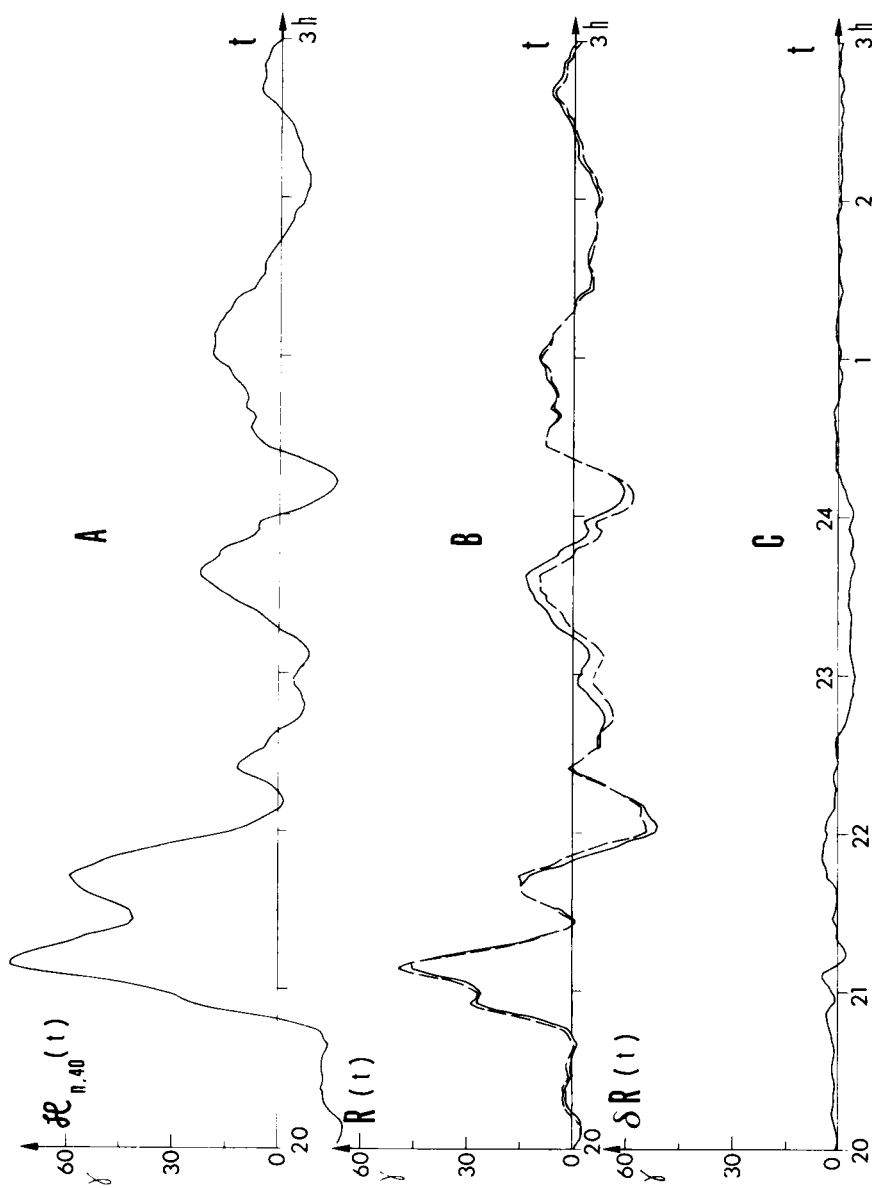
$$\tau \frac{dR(t)}{dt} + R(t) = S(t), \tag{7}$$

where τ is an unknown time constant and $S(t)$ a linear function of the input $H_n(t)$. The induction laws suggest that $S(t) = d\Phi/dt$ with $\Phi = \mathbf{v} \cdot \mathbf{H}_n(t)$, \mathbf{v} being an horizontal vector whose components are α and β .

As $H_n(t)$ and $R(t)$ are digitized with a sample rate T , τ , α and β must verify the following system

$$R[(n - 1) T] = \frac{2\tau + T}{2\tau - T} R(nT) + \frac{\alpha}{2\tau - T} [H[(n - 1) T] - H(nT)] + \frac{\beta}{2\tau - T} [D[(n - 1) T] - D(nT)] \tag{8}$$

for $n = 1, 2, \dots, N$, N being the number of points of the observed time series. The system (8) is obtained by taking the z transform of (7) – the operator d/dt being estimated by $(2/T)[(1 - z)/(1 + z)]$.



Oct. 8, 1975

Oct. 9, 1975

Figure 5. Example of reconstruction of the normal horizontal field projected on the direction 40° E of north with the average impulse response deduced from Fig. 4. From top to bottom: A - projected normal field $H_{n, 40^\circ}(t)$; B - continuous line is the observed anomalous field $R(t)$; dashed line is the predicted anomalous field $R'(t)$; C - difference between the predicted and the measured anomalous field $R'(t) - R(t)$.

In practice, $R(t)$ is only known to within a weak additive constant (Babour & Mosnier 1976); however, in equation (7), the actual value of $R(t)$ is assumed to be known. So, we have to introduce, for every sample, the average value of $R(t)$ as an additional unknown parameter in (8). This system is then solved using least-square techniques. The value of τ is the time constant of the system governed by (7), $\tan^{-1}(\alpha/\beta)$ gives the direction most effective for induction (Δ), $(\alpha^2 + \beta^2)^{1/2}/\tau$ is the magnification factor of the dynamic system.

For the computation of the parameters τ , α , β the time series have been previously filtered using linear Butterworth filters described above. The results are independent of the sampling interval T . Table 2 gives the results for the three samples in the period range 1200–5400 s.

Table 2.

| No. | τ s | $(\alpha^2 + \beta^2)^{1/2}$ s | $\theta = \tan^{-1}(\beta/\alpha)$ |
|-----|----------|--------------------------------|------------------------------------|
| 1 | 741 | 666 | 40° |
| 2 | 793 | 755 | 33° |
| 3 | 776 | 772 | 39° |

The values obtained for parameters τ , α , β are in good agreement. The direction $\theta = \tan^{-1}(\beta/\alpha)$ is very close to the direction found previously. Solving equation (7) with mean values of parameters ($\tau = 775$ s, $(\alpha^2 + \beta^2)^{1/2} = 736$ s, $\theta = 37^\circ$) a predicted output $R'(t)$ can be obtained and compared to the actual $R(t)$ series (Fig. 6). The agreement between $R(t)$ and $R'(t)$ is very good.

4 Comparison of the estimated transfer functions

The validity of the results obtained in the time domain has been verified through the comparison between the observed time series $R(t)$ and the predicted ones. From these results, two estimates of the transfer function between $R(t)$ and the projected normal field have also been obtained. These two estimates are compared to the previous one obtained in the frequency domain. Fig. 7 shows the estimated transfer functions (real and imaginary parts) obtained using these three methods:

- (i) TF , obtained through the spectral analysis, is the arithmetic average of the curves of Fig. 3 corresponding to the three samples;
- (ii) W , is the Fourier transform of the average impulse response deduced from Fig. 4;
- (iii) F , arises from the functional relation (7). Its analytical expression is

$$F(f) = (\alpha^2 + \beta^2)^{1/2} (2i\pi \cdot f) / (1 + 2i\pi \cdot f\tau). \tag{9}$$

Mean values of parameters τ , α , β have been used.

The agreement between the three curves is quite good both for real and imaginary parts. However, for shorter periods (less than about 800 s), a discrepancy can be noted and can be explained by the following remarks:

- (i) for this frequency range, the spectral power is low and the spectral estimates may be erroneous;
- (ii) the Fourier transform of the impulse response of Fig. 4 is not accurate for higher frequency;
- (iii) the curve labelled F was obtained with filtered data using a band pass filter attenuating high-frequency components.

Nevertheless, for periods less than 1200 s the differences between the three estimated real parts of the transfer function are about 10 per cent and reach at most 30 per cent for

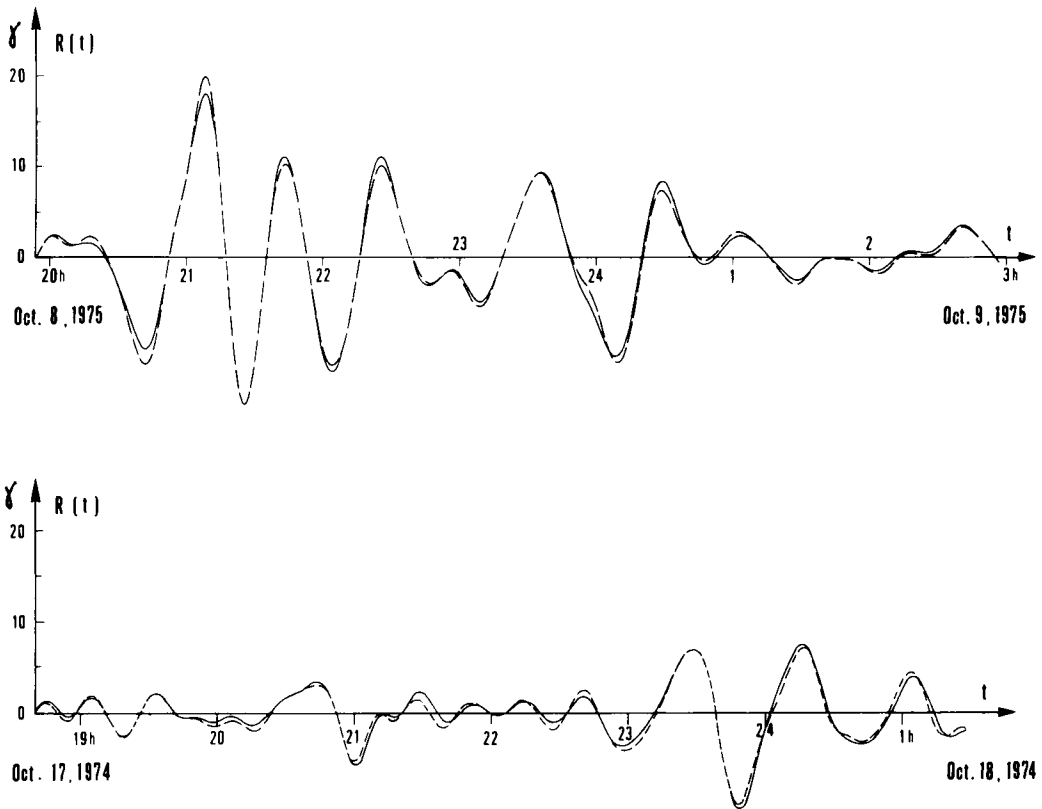


Figure 6. Comparison of the observed anomalous field $R(t)$ (continuous line) with the predicted anomalous field $R'(t)$ (dashed line) obtained through integration of equation (7) with $\tau = 775$ s, $(\alpha^2 + \beta^2)^{1/2} = 736$ s, $\theta = 37^\circ$. The time series have previously been filtered for the period band 1200–5400 s. The top figure is for sample 2 and the bottom one is for sample 3.

shortest periods (600 s). The same agreement can be noticed for the estimated imaginary part at least for period lower than 1000 s. This comparison gives a further confirmation that the functional relation (7) is a good approximation of the relation between the normal and the anomalous field in the period range 1200–5400 s.

5 Conclusion

5.1 INTERPRETATION OF THE TRANSFER FUNCTION

The modulus of the transfer function for the anomalous field at the particular station, Durban (Fig. 3), reaches values close to unity or even greater for period lower than 25 min. For stations nearer to the maximum of the anomaly, this modulus would be even greater. This high value gives a further confirmation for the hypothesis of current concentration: fields of this magnitude cannot arise from a local induction in an elongated structure.

In fact, this transfer function yields information about the deep structure of the remote area where the currents are induced. Although this area cannot be explicitly located, it seems reasonable to assume that these currents are induced in the ocean: the conductivity of the sea water is high and the region where the anomaly is observed is connected to the Mediterranean Sea and to the Atlantic Ocean.

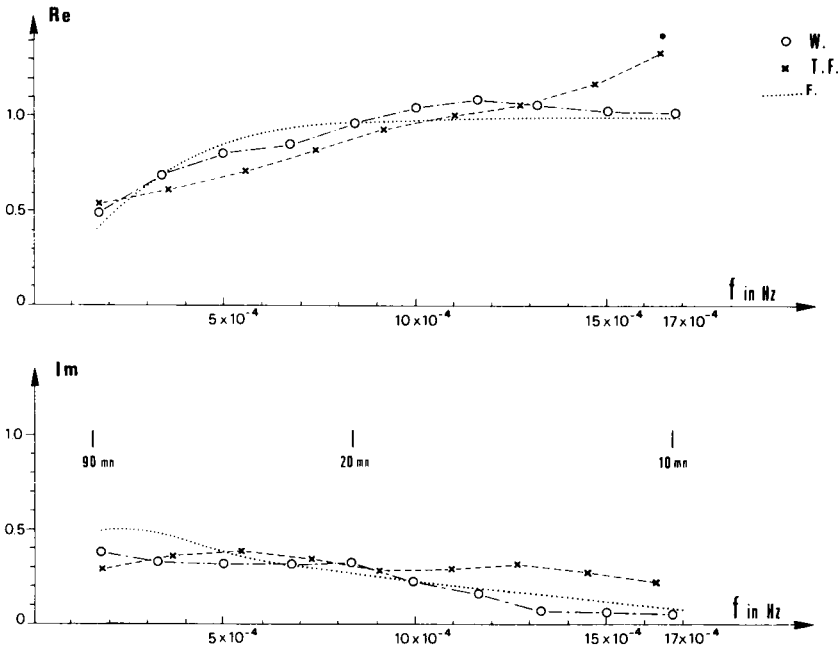


Figure 7. Comparison of the three evaluation of the transfer function as a function of frequency: *TF* is the evaluations deduced from spectral estimates; *W* is obtained from the Wiener filter; *F* is the transfer function deduced from relation (7).

Using this assumption and supposing that the currents behave like direct ones in the region where they are concentrated, the time variation of these induced currents must be the same as that of the observed anomalous field $H_a(t)$ generated by their concentration. Therefore the complex transfer function relating the anomalous field to the normal one is proportional to within a real multiplicative constant, to the ratio E/H between two cross components of the electromagnetic field inside the region where the induction takes place.

From this point of view, the differential equation (7) may be given an interesting interpretation: let us assume that the induction takes place in a stratified medium with a thin conductive layer – conductivity σ , thickness δ – an insulating layer till depth z_0 and a perfectly conducting substratum below this depth. The relationship between two cross components of the electric and magnetic field is given, in the frequency domain by (Schmucker 1970):

$$E/H = (2i\pi f \mu_0 z_0) / (1 + 2i\pi f \mu_0 z_0 \sigma \delta). \tag{10}$$

The current flowing in the thin layer – which stands for the ocean – is proportional to E ; from the above assumption, it is one component of this current which gives rise to the anomaly through a concentration process.

The transfer function arising from the differential equation (7) which relates the anomalous field to the normal one is given by the equation (9) which has the same form as the equation (10). Taking into account the previous assumptions, the two relations (9) and (10) can be identified to within a multiplicative constant. In particular, a comparison of the real and imaginary parts leads to $\tau = \mu_0 z_0 \sigma \delta$; taking into account the computed value of τ and assuming for σ a value of $4 \Omega^{-1} m^{-1}$ and for δ a value of 3 km (mean depth of the ocean), we find $z_0 \approx 50$ km.

5.2 GEOPHYSICAL INTERPRETATION

We have pointed out the close relationship between the couple $[H_{n,40^\circ}(t), R(t)]$ and that constituted by two perpendicular components of the electromagnetic field over the area where induction occurs for the observed phenomena. For this area, we are led to propose a plane-layered model including a perfectly conducting medium at a depth of 50 km. Such a high conducting layer has often been involved from magnetotelluric measurements and from geomagnetic depth sounding (Fournier 1970; Schmucker 1973; Gough 1973), the different estimates of its depth vary from some tens to several hundreds of kilometres. Nevertheless, we must recall that this conducting layer is related to the area where the induction takes place and not to the area where the anomaly is observed.

We have now to explain the stable direction most effective for induction, this direction being different from the direction perpendicular to the currents flowing in the area of the anomaly. Owing to its stability, we will investigate whether the geometrical characteristics of the area where induction takes place can account for this direction (Δ). The previous considerations led us to locate this unknown area over oceanic regions: Mediterranean Sea and Atlantic Ocean. Therefore, we have to look among the geometrical characteristics of this area, for the features which can deflect the currents toward the area where the anomaly is observed.

In addition to its borders, the geometry of the Atlantic Ocean is characterized by an elongated north–south structure, the mid-Atlantic ridge, which probably modifies the distribution of conductivity. This structure seems too far from the observed anomaly to account for the observed concentration of current. The only major feature whose geometry may explain the direction (Δ) seems to be the transition ocean–continent, i.e. the continental margin. This transition corresponds to conductivity variations at two different levels:

(i) Superficially, the transition ocean–continent corresponds to a conductivity contrast reaching several orders of magnitude. The particular geometry of the conducting medium – ocean: Bay of Biscay at the west and Bay of Lion at the east – might deviate the currents induced in the ocean and filter those which are induced by some particular direction of the external magnetic field. Preliminary attempts of three-dimensional modelling, taking into account a simplified model geometry of the continents have proved that such an explanation is a realistic one (Weidelt 1975 and private communication). Besides, the sedimentary basin of Aquitaine can explain an electric link between the Atlantic Ocean and the region of the anomaly.

(ii) At greater depth, the continental margin involves a transition between the oceanic crust and the continental one. Owing to heat-flow measurements, we know that the isothermal surfaces come nearer to the surface for the oceanic lithosphere. Thus, continental margins appear to correspond to three-dimensional inhomogeneities of conductivity. Such structures are able to deviate – in the same way that the superficial ocean–continent transition, and with the same geometry – deep currents toward the observed anomaly, if this anomaly is electrically connected to these deep conducting layers.

Considering the measurements at our disposal, and the period range under study (600–5400 s), we cannot exclude these deepest currents and both processes may account for the observed anomaly. The evaluation of the importance of these two processes needs an extension of the period range to study.

So, the study of the temporal relation between the anomalous field and the normal one has allowed to propose a model which seems to be associated to an oceanic lithosphere including a conducting layer at a depth of 50 km. A quantitative discussion of the physical

mechanisms responsible for the concentration of currents will form the object of a forthcoming paper.

Acknowledgments

The authors are very indebted to Professor Schmucker and Dr Weidelt for valuable discussions and for the model computations performed. Thanks are due to Dr Le Mouel and M. Daignières for their assistance during the progress of this work. This work was supported by Institut National d'Astronomie et de Géophysique through 'Action Thématique Programmée: Géodynamique de la Méditerranée Occidentale'.

Contribution CGG No. 196; Contribution IPGP No. 225.

References

- Babour, K., Mosnier, J., Daignières, M., Vasseur, G., Le Mouel, J. L. & Rossignol, J. C., 1976. A geomagnetic variation anomaly in the northern Pyrenees, *Geophys. J. R. astr. Soc.*, **45**, 583–600.
- Babour, K. & Mosnier, J., 1976. Differential geomagnetic sounding, *Geophysics*, in press.
- Cochrane, N. A. & Hyndman, R. D., 1970. A new analysis of geomagnetic depth sounding data from western Canada, *Can. J. Earth Sci.*, **7**, 1208–1218.
- Fournier, H. G., 1970. Contribution au développement de la méthode magnétotellurique, notamment en vue de la détermination des structures profondes, *Thèse*, 3 vols, 320 pp., Faculté des Sciences de Paris, Paris.
- Gough, D. I., 1973. The geophysical significance of geomagnetic variation anomalies, *Phys. Earth planet. Int.*, **7**, 379–388.
- Jenkins, G. M. & Watts, D. G., 1968. *Spectral analysis and its applications*, 525 pp, Holden-Day, San Francisco.
- Rikitake, T., 1966. *Electromagnetism and the earth interior*, 308 pp, Elsevier, Amsterdam.
- Schmucker, U., 1970. Anomalies of geomagnetic variations in the south-western United States, *Bull. Scripps Inst. Oceanogr.*, **13**, 1–165.
- Schmucker, U., 1973. Regional induction studies: a review of methods and results, *Phys. Earth planet. Int.*, **7**, 365–378.
- Treitel, S. & Robinson, E. A., 1966. The design of high resolution digital filters, *I.E.E. Trans. Geosci. Electron.*, **GE4**, 25–28.
- Souriau, M., 1974. Acquisition et traitement des données numériques pour les grands profils sismiques, *Thèse*, Université Paris VI, Paris.
- Weidelt, P., 1975. Electromagnetic induction in three dimensional structures, *J. Geophys.*, **41**, 85–109.